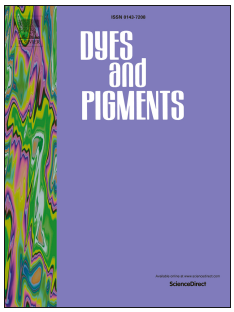

A physically grounded model for predicting subtractive colour mixing: towards a perception-independent framework

Juan Tricas-Ranchal, Antonio Molina, Ana Sanchez-Cano, Elvira Orduna-Hospital, Justiniano Aporta

PII: S0143-7208(25)00610-2

DOI: https://doi.org/10.1016/j.dyepig.2025.113240

Reference: DYPI 113240

To appear in: *Dyes and Pigments*

Received Date: 16 July 2025

Revised Date: 24 August 2025

Accepted Date: 12 September 2025

Please cite this article as: Tricas-Ranchal J, Molina A, Sanchez-Cano A, Orduna-Hospital E, Aporta J, A physically grounded model for predicting subtractive colour mixing: towards a perception-independent framework, *Dyes and Pigments*, https://doi.org/10.1016/j.dyepig.2025.113240.

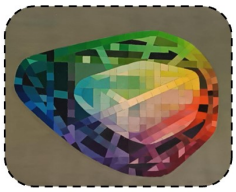

$$G = \frac{\int_{400}^{700} \rho(\lambda) d\lambda}{\int_{400}^{700} d\lambda}$$

$$g(\lambda) = \rho(\lambda) - G$$

$$Ix(G) = \int_{550}^{700} g(\lambda) d\lambda$$

$$Iy(G) = \int_{475}^{625} g(\lambda) d\lambda$$

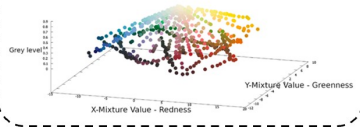

The **methodology** consists in the construction of a high-resolution reflectance database, $\rho(\lambda)$, and the generation of a corresponding **set of colour coordinates** using newly defined physical parameters. Formulating a novel, **perception-independent colour space**, termed the **General Sample Plane** (**GSP**). This framework is further extended into three dimensions as the **General Sample Volume** (**GSV**). Unlike conventional perceptual models, the GSP and GSV are constructed from optical properties alone, with **no reliance on observer-based colour metrics**.

The coordinate system introduced, based on the parameter set $\left(\boldsymbol{G}, \boldsymbol{M_x(G)}, \boldsymbol{M_y(G)}\right)$, derives directly from the $\rho(\lambda)$ curve and supports the computation of a perception-independent space. $\left(\boldsymbol{I_x(G)}, \boldsymbol{I_y(G)}\right)$ are calculated according to the equations in the left. Mixture Values are found by estimating to a quadratic curve the data for $I_X(G)$ or $I_Y(G)$ against G and projecting the points into a line tangent to the curve at white point.

The reflectance-based calculation process developed for opaque paints on canvas enabled the construction of a linear, perception-independent representation system for subtractive mixing. In **two dimensions**, the **GSP**, and in **three dimensions**, the **GSV.**

Title: A physically grounded model for predicting subtractive colour mixing: towards a perception-independent framework

Authors: Juan Tricas-Ranchal, Antonio Molina, Ana Sanchez-Cano*, Elvira Orduna-Hospital, Justiniano Aporta

Applied Physics Department, University of Zaragoza, 50009 Zaragoza, Spain

*Corresponding author anaisa@unizar.es (A. Sanchez-Cano)

Abstract

This work develops a physically grounded model for predicting pigment mixture colours that operates independently of visual perception. The central objective is to identify intrinsic, measurable parameters that enable accurate and linear predictions of colour outcomes, validated through a dataset of 8421 manually prepared samples, including 43 base pigments and their binary mixtures, both inter-pigment and pigment-white.

To achieve this, three interconnected goals are pursued. First, the construction of a high-resolution reflectance database, $\rho(\lambda)$, and the generation of a corresponding set of colour coordinates using newly defined physical parameters. Second, the formulation of a novel, perception-independent colour space, termed the General Sample Plane (GSP), in which each pigment sample G is uniquely represented by the triplet $\big(G, M_x(G), M_y(G)\big)$. This framework is further extended into three dimensions as the General Sample Volume (GSV). Unlike conventional perceptual models, the GSP and GSV are constructed from optical properties alone, with no reliance on observer-based colour metrics. Third, the predictive validity of this coordinate system is evaluated by analysing the linearity of trajectories traced by pigment mixtures and their respective whitening stages in the GSP. The results confirm that mixtures of two components, both pigment-pigment and pigment-white, describe highly linear paths in this space (reaching $R^2 > 0.99$), with minimal chromatic distortion even across broad spectral domains. Additionally, quantitative evaluation of interpolation accuracy, based on excluded intermediate mixtures, showed low ΔE values ($\Delta E \leq 1.0$) in the GSP space, where ΔE represents the Euclidean distance between predicted and measured coordinates, confirming the model's reliable predictive performance. The model offers a scalable, quantitative basis for physically consistent colour prediction in subtractive systems, with potential applications in pigment formulation, digital calibration, and optical modelling of coloured materials.

Keywords: Subtractive colour mixing, Pigment mixtures, Physically based colour space, Reflectance modelling, Perception-independent colour prediction, Whitening trajectories, Colour formulation

1. Introduction

Throughout history, both researchers and artists have faced significant challenges when mixing pigment colours and attempting to accurately represent them. Often, different results were obtained even when following supposedly identical methodologies, highlighting a persistent issue in colour prediction for opaque media. Predicting the colour of mixed opaque pigments and dyes relies primarily on the turbid media theory proposed by Kubelka-Munk (K-M) in 1931 and latterly expanded [1–3]. This theory models the optical behaviour of light within a scattering layer, such as paint, through two fundamental optical constants: an absorption coefficient (K) and a scattering coefficient (S). These constants, together with coating thickness and substrate reflectance, allow for the quantification of the optical response of the material [1–3]. It is commonly assumed that the absorption and scattering coefficients of a mixture can be estimated from those of its components using an additive and scalable model [4]. The use of K-M theory in predicting the spectral reflectance factor of an opaque specimen from its constituent optical constants is well established in practice and widely documented in the literature [1–3,5–7]. Its practical success is largely due to the reduction in mathematical complexity when dealing with opaque samples, the elimination of thickness control, and extensive empirical validation across a wide range of materials.

Current colour prediction models for pigments, including those based on K-M, rely on the absorption and scattering properties of the pigment molecules. However, these models are often strongly dependent on the specific characteristics of the pigments and binders used and commonly neglect the substrate under the assumption of a sufficiently opaque layer. This necessitates the consideration of many parameters to ensure reproducibility [4]. Several methods have been developed to determine the K-M optical constants from spectrophotometric measurements, including the black-white, infinite, masstone-tint, and two-region methods [4]. In particular, the two-region method has been enhanced to automatically identify opaque spectral regions using the masstone-tint approach. More advanced approaches, such as the single-constant Kubelka-Munk theory with impurity index (1p-KM) theory, which introduces the *impurity index p*, a spectrally non-selective scattering property for each chromatic component, to improve linear mixing models and extend their applicability to a broader range of pigment concentrations, including pure colours [8]. Prediction results remain more accurate for opaque mixtures compared to other sample types due to the variability in film thickness and the intrinsic limitations of K-M theory [4].

A key unresolved issue in pigment mixing is the lack of linearity observed in subtractive systems, in contrast to additive colour systems [9]. When using tristimulus values, an illuminant, and reflectance spectra $\rho(\lambda)$, the trajectories formed by binary pigment mixtures in colour spaces are often unpredictable curves. This nonlinear behaviour is evident in the International Commission on Illumination (CIE) diagrams (e.g., $CIExyY$ or $CIEL^*a^*b^*$) when modelling subtractive mixtures in opaque matte pigments [10–13]. Existing systems limit the prediction of pigment blends to small or proximal regions where these curved trajectories can be locally approximated as linear [7].

In contrast to empirical and material-property-based models, progress has been made in molecular-level colour prediction, especially for dyes. Computational approaches such as Density Functional Theory (DFT) and Time-Dependent DFT (TD-DFT), along with vibronic coupling treatments, have been used to simulate spectral features (e.g., peak position, shape, and intensity) of rigid dyes in solution [14]. These first-principles methods simulate spectral features quantitatively, showing high accuracy in predicting UV-VIS spectra and colour coordinates [15] and have even been applied to study natural dyes such as madder and its glycosidic forms, which are difficult to experimentally characterize. However, real materials also present challenges related to temporal stability, such as photodegradation

of dyes and pigments, a ubiquitous phenomenon influenced by factors such as irradiance (intensity and wavelength), oxygen presence, temperature, catalysts, dye concentration, solvent or substrate type, humidity, and mordants, is an active area of research. Understanding these parameters is crucial for accurate prediction and long-term preservation of colour, particularly in the context of cultural heritage [15].

The theoretical framework underlying this study was initially presented by the authors (A.M. and J.A.) at previous conferences [16,17]. These preliminary results addressed the intrinsic unpredictability of subtractive colour mixing. The present work extends this foundation by providing the first empirical validation of the model using a high-resolution spectral dataset of over 8000 samples. Additionally, it formally defines the General Sample Plane (GSP) and General Sample Volume (GSV) coordinate systems, and evaluates their predictive accuracy and linearity in both whitening and binary pigment mixtures.

The primary aim of this work is to develop a mathematical model for predicting pigment mixture colours that does not rely on visual perception. Specifically, the study seeks to identify physically derived parameters capable of enabling linear colour predictions and to experimentally validate the model through a systematic analysis of 43 base pigment samples and their binary mixtures, both with each other and with a standardized white reference pigment, resulting in a dataset of 8421 manually prepared samples. To achieve this, the research pursues three interconnected objectives. First, to construct a comprehensive database of $\rho(\lambda)$ and organize the corresponding colorimetric data for all 8421 samples based on newly defined coordinates and calculated parameters. Second, to establish a novel, perception-independent system for representing colour, defined both in two dimensions, GSP, and in three dimensions, GSV. That, unlike conventional perceptual systems tied to human visual response, is entirely grounded in measurable optical behaviour. Third, to experimentally evaluate the proposed coordinate system by assessing the linearity of colour trajectories derived from mixtures, thereby testing its predictive capability. The anticipated result is a colour representation framework that remains independent of human perception while improving the accuracy and linearity of pigment mixture modelling. In contrast to traditional models, where predictive accuracy diminishes over broader chromatic ranges due to the curvature of colour-mixing paths in perceptual spaces, the GSP and GSV are designed to maintain linearity across a wider gamut, providing a physically consistent alternative for colour prediction in opaque, subtractive media.

2. Materials and Methods

This study involved the preparation and analysis of a comprehensive dataset comprising 8421 hand-painted samples of opaque pigment mixtures applied on canvas. Each sample measured approximately 5 × 7 cm and was painted manually using consistent techniques, covering a total area of around 30 m^2. To ensure consistency across the 8421 manually prepared samples, a strict and standardized protocol was followed during sample preparation. Each mixture series was created by defining ten discrete steps based on volumetric ratios between the components (e.g., pigment-pigment or pigment-white), with volumetric increments of 10%. Mixing was performed using graduated precision pipettes to ensure accurate volumetric proportions at each step. Homogenization was achieved by blending each mixture for three minutes using a mechanical stirrer. Samples were applied manually with flat synthetic brushes of uniform width (30 mm), using a single horizontal stroke technique repeated three times to ensure even coverage. Drying conditions were maintained in a controlled environment at 22 °C ± 1°C and 45% relative humidity for 24 hours. To verify reproducibility, repeated measurements of reference samples across multiple batches were conducted. The standard deviation in reflectance values across these

replicates remained within ±1.5% throughout the 400-700 nm spectral range, confirming the statistical consistency and reliability of the dataset. The set of samples was structured into several categories to allow both systematic exploration and empirical validation of the proposed colorimetric model. The first group included 43 base samples, each corresponding to a distinct commercial pigment. A second group comprised 416 white-tinted samples produced through progressive mixing of each base pigment with a standard white pigment in nine discrete steps. The third group, the largest, consisted of 6210 binary pigment mixtures and associated gradations, with each step also blended with white to assess spectral behaviour under tinting. Finally, 1752 samples were generated to analyse intermediate mixtures and address the theoretical challenge of linearizing multi-step subtractive combinations in the proposed framework.

Spectral reflectance measurements, from 400 to 700 nm, were conducted using a Konica Minolta CM-700d (Konica Minolta Sensing Inc., Osaka, Japan) operating under standard conditions, in this case, 8°/specular component included. Data acquisition and processing were performed via the proprietary Spectramagic™ NX software v3.40. For darker samples, whose reflectance values fell near or below the instrument's uncertainty threshold (2%), a StellarNet Black Comet spectroradiometer (StellarNet Inc., Tampa, Florida, USA) was used in conjunction with an integrating sphere and a xenon arc lamp to ensure accurate radiometric measurement, and spectral data were compared with the previous results to minimize measurement errors. To increase the initial spectral sampling resolution from 10 nm to 0.01 nm in the measured wavelength range, linear interpolation was applied using the *interpolate.interp1d* method from the SciPy library. The interpolated data enabled high-accuracy numerical integration via the trapezoidal rule, used to calculate integrated parameters from the $\rho(\lambda)$.

Data handling was performed using Microsoft® Excel 2024 (Microsoft Corporation, Washington, USA) for initial organization and labelling. Numerical integration, coordinate calculation, and spectral interpolation were implemented using a custom codebase in Python in Visual Studio Code (version 1.88). Graphical output was rendered using GNUplot (version 5.4.8, T. Williams et al., USA), and colour-space modelling was conducted with Blender (version 4.2.8, Blender Foundation, Amsterdam, The Netherlands) and Unreal Engine (version 5.5.4, Epic Games, Cary, USA), which allowed the generation of both planar and volumetric visualizations of the colour datasets.

3. Mathematical model formulation

Three key parameters were defined from the $\rho(\lambda)$ of the coloured samples, with a white sample considered as the pivotal centre of the model. First to all, analogous to the role of lightness in perceptual theories, this model introduces a foundational parameter that serves as one of the coordinates in its three-dimensional framework and forms the basis for deriving all other values.

The Grey Level (G) represents the normalized spectral whiteness of each sample and is calculated as the integral of the reflectance between 400 and 700 nm, divided by the bandwidth. The Graphical Intensities $\left(I_{\mathrm{x}}(G), I_{\mathrm{y}}(G)\right)$ correspond to signed integrals of the difference between the sample's reflectance curve and its G baseline, over specific wavelength regions (550-700 nm for $I_{\mathrm{x}}(G)$, 475-625 nm for $I_{\mathrm{y}}(G)$). These were chosen to capture chromatic variation orthogonal to G.

From these values, Mixing Values $\left(M_{\mathrm{x}}(G), M_{\mathrm{y}}(G)\right)$ were derived using second-order polynomial fits constrained to pass through the white reference point in each series. By projecting each pigment's

gradation curve (e.g., from a colour mixed progressively with white) onto a common linear path defined by the white point, obtained coordinates with demonstrably linear behaviour. This procedure enabled the construction of a novel two-dimensional colour representation space, GSP, and its three-dimensional extension, GSV, by incorporating G as a third dimension. These constructs were conceived to replace perception-based colour spaces with a model rooted in physically measurable optical parameters.

3.1. Grey level

This coordinate, G, quantifies the spectral lightness of a sample. It is calculated by integrating the normalized reflectance spectrum $\rho(\lambda)$ over the range 400-700 nm, as defined by the measuring device, and normalizing it to the theoretical maximum, an ideal white with constant unit reflectance.

Conceptually, it reflects the proportion of spectral energy reflected by the sample compared to that of a perfect white, as shown in (Eq. 1).

$$G = \frac{\int_{400}^{700} \rho(\lambda) d\lambda}{\int_{400}^{700} d\lambda} \qquad \text{(Eq. 1)}$$

This parameter exhibits a notable mathematical property; when G value is treated as a constant spectral function, the difference between the reflectance spectrum $\rho(\lambda)$ and the G function integrates to zero. This implies that the areas above and below the G line cancel each other out, as illustrated in Figure 1, where the spectrum of an arbitrary sample, the G line, and the corresponding areas are shown, along with the equation that expresses this cancellation.

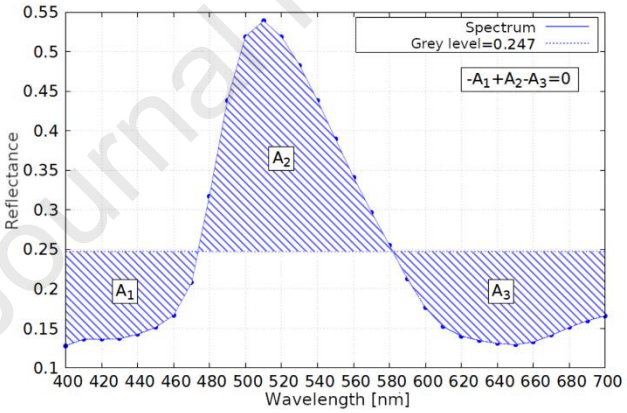

Figure 1. Illustration of the spectral lightness coordinate G as a constant function. The reflectance spectrum $\rho(\lambda)$ of an arbitrary sample is shown alongside the horizontal G line. The shaded areas, shown in striped blue above and below the G line represent regions where the spectrum exceeds or falls below G, respectively. These areas are equal in magnitude, demonstrating that their net integral is zero.

3.2. Graphic Intensity

Subsequently, two additional coordinates, purely dependent on the energy spectrum, are defined as X and Y Graphic Intensities ($I_x(G), I_y(G)$), according to the formulas in **Error! Reference source not found.** and **Error! Reference source not found.**.

$$I_x(G) = \int_{550}^{700} g(\lambda) d\lambda \qquad \text{(Eq. 2)}$$

$$I_y(G) = \int_{475}^{625} g(\lambda) d\lambda \qquad \text{(Eq. 3)}$$

Given that $g(\lambda) = \rho(\lambda) - G$. These parameters could be interpreted as "redness" or "greenness", depending on the spectral regions used for integration. Since the integration is performed over specific wavelength ranges, rather than across the full spectrum as in the previous case, the integrals are not null. The integration limits are flexible and could be modified if a broader spectrum is considered.

At this point, it is essential to define the concept of whitening, understood as the progressive mixture of a pigment with white. This process involves the original colour and nine intermediate steps, which are considered as a series and treated as a whole, rather than as independent samples, even though each one has its own G, $I_x(G)$, and $I_y(G)$ values, Figure 2.

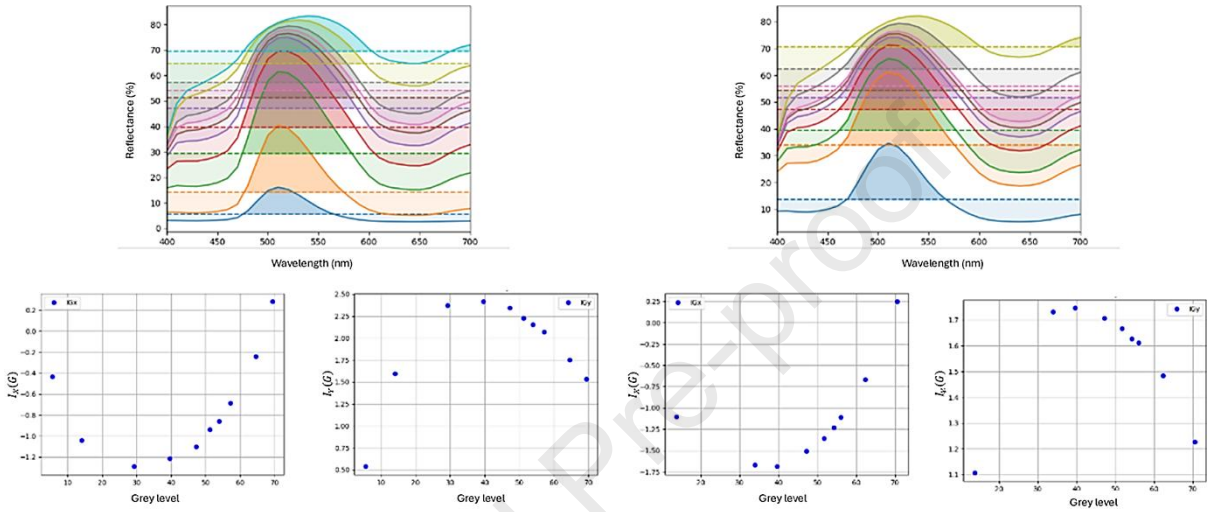

Figure 2. Spectral reflectance curves (top) and corresponding Grey Level vs. Graphical Intensity analyses (bottom) for two sample sets series (left and right). The spectral profiles are grouped for visual comparison, while the scatter plots illustrate the relationship between G and $(I_x(G), I_y(G))$ components derived from the graphical representation.

3.3. Mixture Value

To define the next parameters, the white sample *(W)* needs to be added to each series, as it is essential for computing the subsequent coordinates and serves as a reference point for the entire mathematical model, with $G = G_W$ and (I_x^W, I_y^W).

These new parameters to be defined extend the previous integrals to state the X and Y Mixture Value (M_x and M_y) through an estimation process.

Specifically, M_x is calculated by plotting $I_x(G)$ against G for the whitening steps and fitting the data to a quadratic curve $Q_x(G)$, Eq. 4, constrained to pass through the reference white point with fixed $(Q_x(G_W), Q_y(G_W)) = (I_x^W, I_y^W)$.

$$Q_x(G) = a_x G^2 + b_x G + c_x \qquad \text{(Eq. 4)}$$

Similarly,

$$Q_y(G) = a_y G^2 + b_y G + c_y \qquad \text{(Eq. 5)}$$

This defined constraint to the W point is necessary to compute the tangent line T_x to $Q_x(G)$ at $G = G_W$, as follows, Eq. 6:

$$T_x(G) = Q_x(G_W) + Q_x'(G_W)(G - G_W) \qquad \text{(Eq. 6)}$$

Similarly, for $T_y(G)$ from $Q_y(G)$.

For each whitening step G, the final M_x values are obtained projecting the point $I_x(G)$ orthogonally onto the tangent line T_x, and the resulting scalar projection ($Proj$) defines $M_x(G)$. The same process is needed to obtain $M_y(G)$, finally obtaining the searched coordinates:

$$(M_x(G), M_y(G)) = (Proj_{Tx}\ (I_x(G), Proj_{Ty}\ (I_y(G)) \qquad \text{(Eq. 7)}$$

These new values are used to represent the position of each step in the whitening process, relative to the reference W, along the tangent as geometrically meaningful direction, Figure 3. It is northwardly that to obtain a dimensionless value, a normalization factor, with the appropriate units, is introduced and applied in the calculations to ensure dimensional consistency.

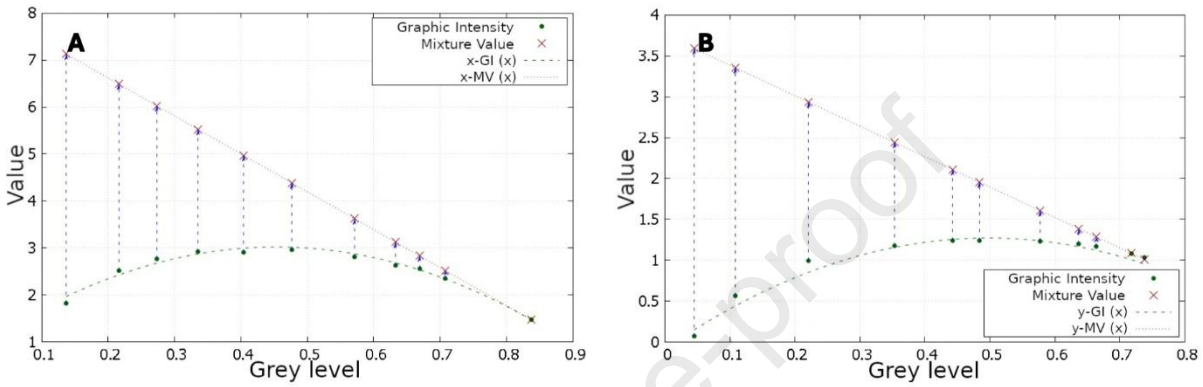

Figure 3. Calculation of Mixture Value (M) in the x- (A) and y-dimensions (B) for arbitrary whitening series. Graphic Intensity (I) values (green dots) are plotted against G for both dimensions. Mixture Values (brown crosses) are computed using the projected I coordinates (purple arrows) derived from the spectrum. Green dotted line represents the quadratic estimation, brown one the tangent to the white point and blue one is the line in the arrow.

It directly follows that $(G,\ M_x(G),\ M_y(G))$ exhibit linear relationships with each other for each whitening series. This triplet is defined as the set of parameters required to characterize pigment colour and to predict linear whitening, with the reference white serving as the centre of the mathematical model.

The quadratic equations obtained from the estimations are not significant in themselves; they are merely used to compute the tangent lines at specific points. The fitted parameters hold no intrinsic relevance beyond this computational role. The next step is to verify whether the linear relationship, clearly observed in the whitening series, also emerges in pigment mixtures, where no mathematical behaviour has been imposed.

4. Data analysis and model validation

The initial measurements consisted of recording the $\rho(\lambda)$ of the 43 base colours and their corresponding whitening series, created by progressively adding white pigment in 10% increments (nine steps, plus the original colour and pure white), Supplement 1. The measurement process adhered to a structured sequence, beginning with three repeated measurements of every of the base colours, first step of each mixture, followed by its corresponding whitening stages, and then proceeding consecutively to the next step in the series. To attempt measurements of the darkest colours, indigo blue as example, control measurements were performed when needed with a more accurately device, as it is previously stated. After measuring the 8421 samples, the data was organized in folders for

subsequent numerical analysis, carried out using a custom code developed for this purpose, and data was structured into a matrix for the spectra of each sample.

The colorimeter provided the $\rho(\lambda)$ data at 10 nm intervals, from 400 to 700 nm. To improve the resolution for numerical integration, the data was interpolated to a final resolution of $\Delta\lambda = 0.01\,nm$. The Python function used for this task was interpolate.interp1d, which applies equation (Eq. 8) for linear interpolation after controlling that this method showed no significant difference compared to higher-order polynomial interpolation methods.

$$f(x|x_1; x_2) = f(x_1) + \frac{f(x_2)-f(x_1)}{(x_2-x_1)}(x - x_1) \qquad \text{(Eq. 8)}$$

A computational loop was written to process the whitening spectra and compute the G value via the trapezoidal integration method (Eq. 9). The resulting integral was normalized by dividing by the theoretical maximum reflectance integral over the 400–700 nm spectral range, which corresponds to 300 nm width and represents the integral of a unitary reflectance function ($\rho(\lambda) = 1$) across that interval. The same normalization procedure was applied to compute $I_x(G)$ and $I_y(G)$ within their respective spectral ranges, as defined in Eq. 2 and Eq. 3.

In these integrals, it is essential to account for the sign: when $\rho(\lambda)$ falls below G, that is, when $g(x) < 0$, the corresponding area is negative; otherwise, it is positive.

$$\int_a^b f(x)dx = \sum_{i=1}^{N} f(x_i)(x_i - x_{i-1}) \qquad \text{(Eq. 9)}$$

Additionally, these quantities were normalized by dividing by 7.5, so that their maximum possible value is 10. This normalization is based on the theoretical limit where $\rho(\lambda) = 1$ for all integrated λ, and $G = 0.5$, which would result in an I_x value of 75. This represents an almost unattainable case, as a step-function spectrum is a purely mathematical construct introduced solely for normalization purposes.

To obtain dimensionless coordinates, this normalization factor is treated as having units of nm, consistent with the wavelength variable, since the units of the integral are the product of the x-axis units (nm) and the y-axis units (dimensionless).

The subsequent step consisted of defining the functions for estimating the M_x and M_y curves through non-linear least squares fitting. The fitting process was constrained by the condition that the curve passes through the I_x^W or I_y^W corresponding to the white colour, which served as a reference shared across all processes, with values obtained from the data analysis. These values were incorporated into the program to ensure proper treatment of the whitening-related inputs. Figure 4 displays the reflectance spectrum of the white sample, $\rho(\lambda)$, with the G value ($G = G_W = 0.83$) indicated by a small, dotted line, Figure 4. The corresponding integral values by areas were $I_x^W = 1.47$ and $I_y^W = 0.64$. It is noted that $I_{x,y}^W = M_{x,y}^W$ since they are being at the common point of the line and the curve, $G = G_W$.

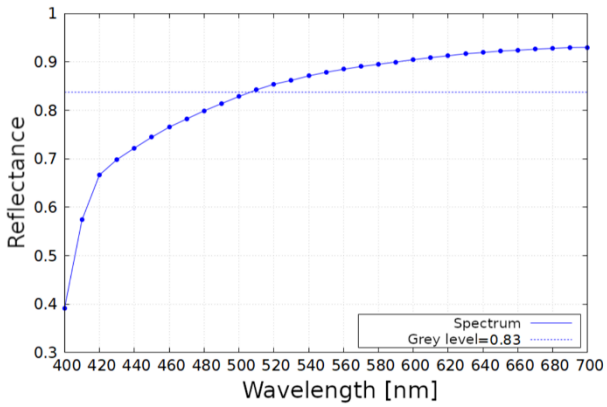

Figure 4. Reflectance spectrum of the white sample. Blue dots represent the experimental reflectance data across wavelengths from 400 to 700 nm, while the continuous line shows the interpolated spectrum. The horizontal dotted line indicates the computed Grey Level (G_W = 0.83), used as a reference in the analysis.

Once the parameter set (G_W, M_x^W, M_y^W) was defined, the analysis proceeded with the characterization of all existing whitening as described in the mathematical model.

At this point, the possibility of subsequent analysis involving mixtures of pigments arises. These mixtures were originally designed to span the largest possible area in the chromatic space, typically by combining three primary pigments (e.g., light green, deep ultramarine violet, and cadmium yellow orange or emerald, light cobalt violet, and cadmium yellow medium).

As an initial example to describe the procedure, a mixture between two greenish colours was analysed; a lighter green tone (sample No. 7, light green pigment), and a darker one (sample No. 9, emerald pigment), as illustrated in Figure 5A. From this mixture, the $\rho(\lambda)$ spectrums were obtained (Figures 5B and 5E), as well as the corresponding $(G, I_x(G), I_y(G))$ integral values, and the $((M_x(G), M_y(G))$ curve estimations for both colours (Figures 5C and 5D for sample number 7 and Figures 5F and 5G for sample number 9).

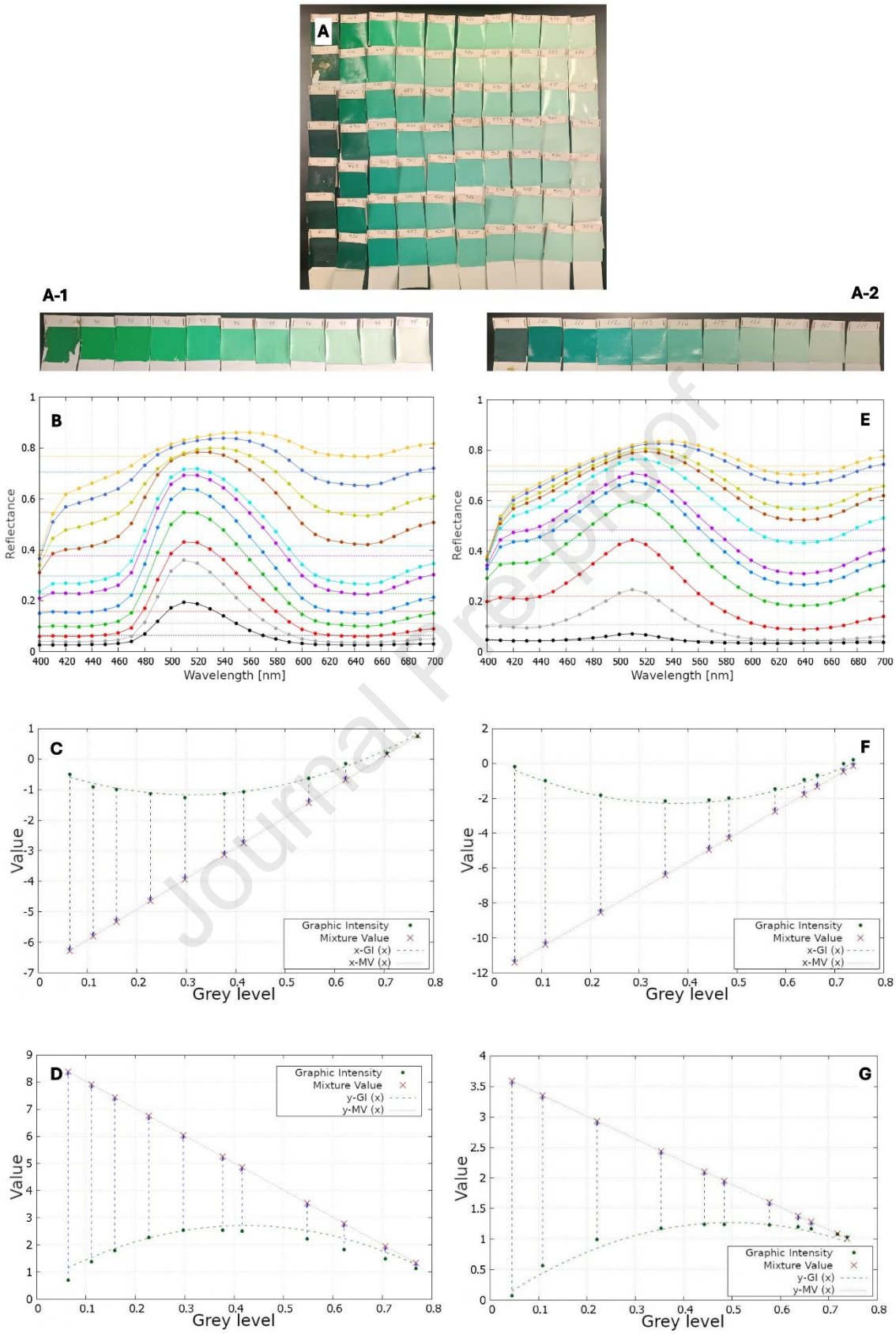

Figure 5. Mixture and whitening analysis between samples 7 (A-1) and 9 (A-2). (A) Photograph of the physical mixture series between samples 7 (top left) and 9 (bottom right), each combined with a whitening agent in increasing proportion from left to right. (B–D) Spectral and graphic analysis of sample 7 with whitening: (B) Reflectance spectra of the mixture series, where

each line corresponds to a different whitening level (same data as in previous figure). (C) and (D) Mixture Value (M) calculations along the x- and y-graphic dimensions, respectively, based on Graphic Intensity (I) values derived from the spectra. (E–G) Equivalent analysis for sample 9: (E) Reflectance spectra of the whitened mixtures. (F) and (G) M calculations in x and y, respectively, following the same procedure as for sample 7.

To generalize the method, the linear and quadratic fitting processes for $(M_x(G),M_y(G))$ were systematically applied at each step of every mixture. For brevity, the figures presented correspond solely to the mixture of base colours 7 and 9, avoiding unnecessary repetition of identical procedures. This process aims to compute the complete set of $\big(G, M_x(G), M_y(G)\big)$ for both the mixture steps and their respective whitening stages. When plotting $M_x(G)$ against $M_y(G)$ for any given colour and its whitening series, the relationship was consistently observed to be linear within the limits of experimental uncertainty. Figure 6A shows how this linear relationship between base samples was achieved through their mixtures, with whitening steps used to assist in calculating the necessary coordinates.

One of the main challenges in this process was establishing a relationship between the different whitening series within a given mixture. To approach this, the $(M_x(G),M_y(G))$ values associated with the first whitening step of each mixture stage are plotted as a basis for the analysis, Figure 6A.

One of the main limitations encountered during the development of this work was that, in the final representation, the whitening series of all the samples obtained from mixtures could not be used directly. Tests showed that linearity was lost when the whitening steps within each mixture were treated as simple extensions of the original base colour whitenings, as illustrated in Figure 6B. This likely occurred because such a representation did not reflect the true nature of the mixture between samples, which was a core requirement of the theory, but rather served as an auxiliary method for calculating coordinates. It was hypothesized that this issue arose from the sequence in which the samples were originally prepared.

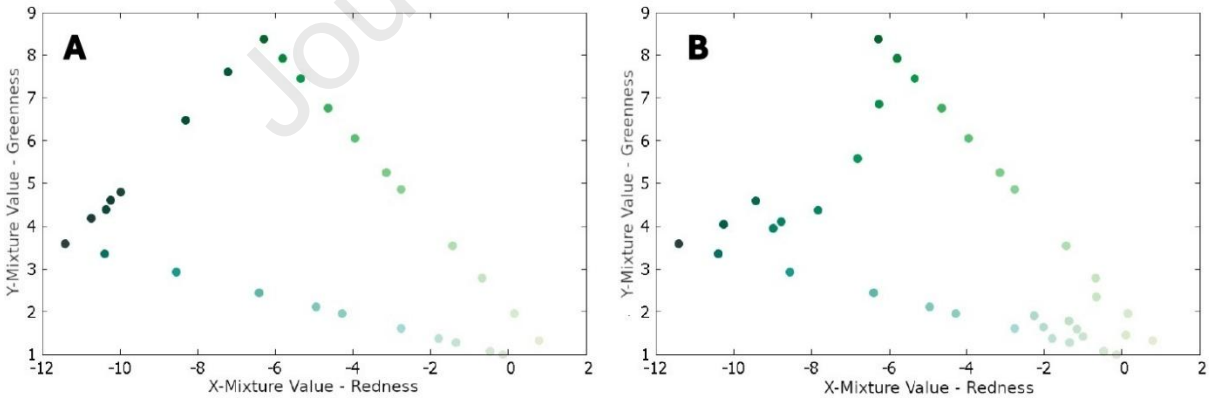

Figure 6. (A) Plot of Mixture Values (M) in the x-dimension against those in the y-dimension, for both the whitening of samples 7 and 9 and their mixture series. The alignment along a straight line demonstrates a linear relationship between M_x and M_y in both cases. (B) Shows the same plot as in (A) but illustrating two whitening steps of the samples in the mixture, proving that validations must be made on the original mixture.

Additionally, the $CIE\ 1931\ xy$ chromaticity coordinates were used for graphical representations and comparative analysis of the colours in both models, the introduced in this paper for subtractive analysis, and the additive widely described in standards [10–13,18]. The same dataset is represented in the $CIE\ 1931\ xy$ chromaticity diagram in Figure 7, where a more complex and less linear behaviour is observed compared to the original GSP space. In GSP, the whitening transitions for both samples are

perfectly linear (R^2 = 1). However, in the $CIE\ 1931\ xy$ perceptual space, the whitening series for sample nº7 shows a decrease in linearity (R^2 = 0.9615), though it improves to R^2 = 0.9772 with a quadratic model. For sample nº9, the drop in linearity is more pronounced, with R^2 = 0.3852 for the linear model, significantly improving to R^2 = 0.9283 with a quadratic fit (an increase of over 140%). The mixture series also exhibits limited linearity (R^2 = 0.5379), which slightly improves under a quadratic model (R^2 = 0.5654), but the best overall performance, however, is achieved by the representation provided in the GSP shown in Figure 6, with an R^2 value of 0.9982. These results highlight the increased nonlinearity of colour behaviour under a perceptual coordinate system and support the use of our models for improved accuracy.

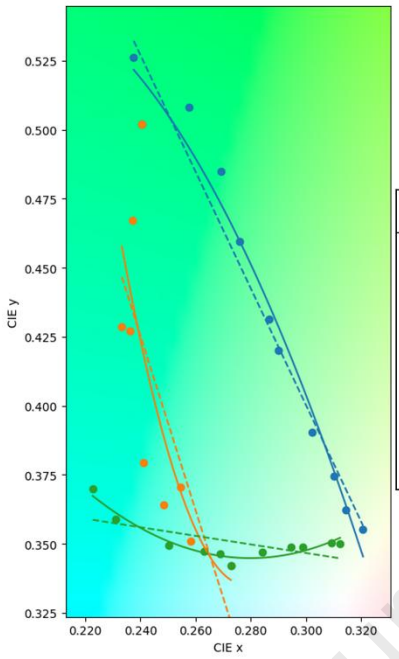

Series	Model Type	Equation	R^2	ΔR^2
Nº7 whitening	Linear	y=-2.111x + 1.034	0.9615	+1.63%
	Quadratic	y=-11.311x² + 4.195x + 0.164	0.9772	
Nº9 whitening	Linear	y = -0.155x + 0.393	0.3852	+140.99%
	Quadratic	y = 6.905x² - 3.864x + 0.886	0.9283	
Mixture	Linear	y = -3.162x + 1.184	0.5379	+5.11%
	Quadratic	y = 61.080x² - 33.971x + 5.059	0.5654	

Figure 7. Visualization of the same sample set from Figure 6A, now plotted in a perception-based colour space (1931 CIE xy). This transformation enables a perceptual comparison of mixtures between samples 7 and 9, revealing differences or improvements introduced by the proposed coordinate system relative to the original spatial layout. Orange points represent the mixture series, while blue and green points depict the whitening transitions for samples 7 and 9, respectively. Linear (dashed lines) and quadratic (solid lines) regression models were fitted to each series in the CIE xy space. Each fit includes its corresponding equation and coefficient of determination (R^2) to assess and compare model performance.

To complete the two-dimensional map of all samples, the remaining base colours and their corresponding whitenings were added, along with additional mixtures, as illustrated in Figure 8, together with an artistical interpretation of the result (painted by A.M.)

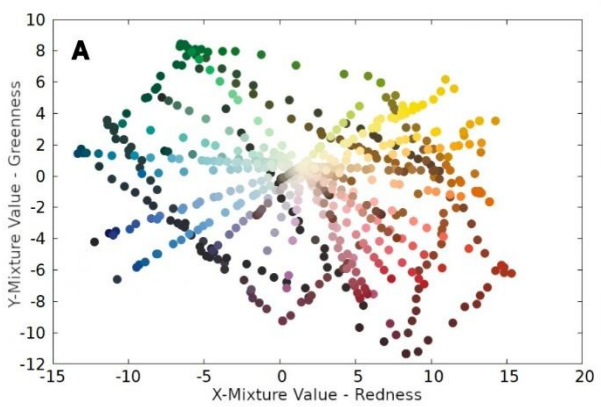

Figure 8. General Sample Plane and its theoretical representation.
(A) General Sample Plane displaying a selection of the measured samples. The layout illustrates the linear relationships observed between different colours through mixing.
(B) Artistic representation of the same plane, drawn according to the initial formulation of the proposed theory. The colours shown correspond to the actual measured samples, providing a visual interpretation of the theoretical structure. This representation shows two horizontal sections of a theoretical Volume, with different G.

To address the problem related to the whitening representations, it would be necessary to repeat each mixture with careful control over this aspect, which would require a significantly larger quantity of white pigment and lead to an increased number of samples, thereby demanding greater time, effort, and material resources. The procedure aims to link the whitening trajectories of the original colours with the corresponding mixtures of their components.

Some mixtures may be difficult to analyse due to the original points being widely separated on the map. This fact highlights the need to construct a three-dimensional volume by taking the $\left(M_x(G), M_y(G)\right)$ plane and adding G as a third orthogonal coordinate. Figure 9 shows the GSV using the same samples as in Figure 8A, while Supplement 2 displays all the samples for completeness. In Supplement 2, $sRGB$ colour coordinates, referenced to the D65 illuminant and the 2° standard observer, were subsequently calculated since they were used for visual colour diagrams, as detailed in standards [10,11,13]. The resulting calculations based on the human visual perception [18] serves exclusively for data visualization on digital screens and does not influence the theoretical computations or the development of the proposed model.

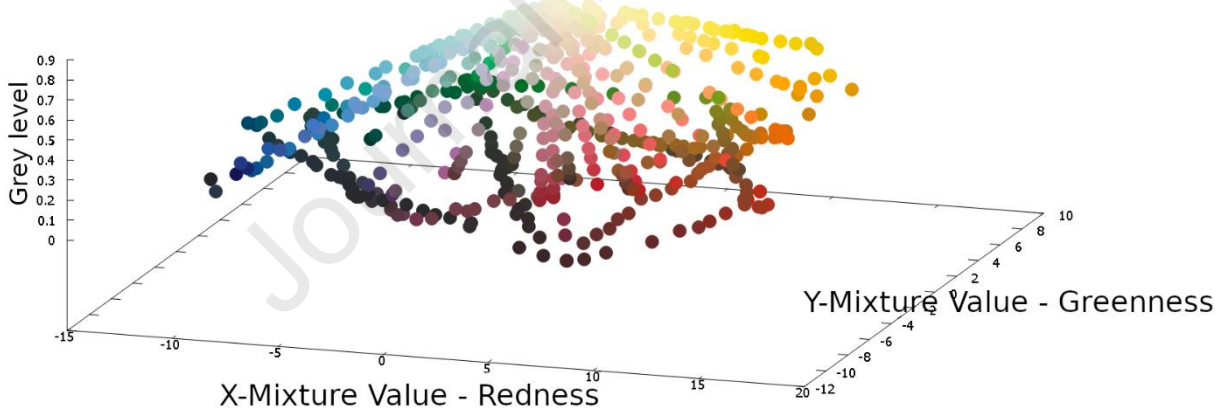

Figure 9. General Sample Volume (GSV) showing the same data as in Figure 8A, plotted in a three-dimensional space defined by redness (X-axis), greenness (Y-axis), and Grey Level (Z-axis). Each point is coloured according to its corresponding sRGB coordinates for visual reference. Shows linear relations between original samples in mixtures and whitenings.

4.1. Interpolation accuracy for unmeasured mixtures

To further assess the predictive capability of the proposed model, an interpolation validation procedure was performed using four representative pigment-white mixtures. For each pigment, a whitening trajectory was constructed, and three intermediate mixture ratios (75:25, 45:55, and 20:80 pigment:white) were deliberately excluded from the fitting process. These excluded samples served as independent validation points. Predicted coordinates in the GSP were obtained by linear interpolation between the two measured endpoints. The predicted $\left(M_x(G), M_y(G)\right)$ values were then compared to their corresponding experimentally measured coordinates using a Euclidean distance metric, defined in Eq. 10:

$$\Delta E = \sqrt{(\Delta \boldsymbol{M}_{\boldsymbol{x}}(\boldsymbol{G}))^2 + (\Delta \boldsymbol{M}_{\boldsymbol{y}}(\boldsymbol{G}))^2} \quad \text{(Eq. 10)}$$

The resulting ΔE values are presented in Table 1. In all cases, the deviations were found to be low, with most ΔE values remaining below or close to a threshold of ≤ 1.00. It is important to note that the ΔE defined in Eq. (10) is not a perceptual colour-difference metric as defined by CIE standards, but instead represents the Euclidean distance between predicted and measured coordinates in the GSP space. This threshold of ΔE ≤ 1.00 corresponds to the average interval of the discrete mixing steps used in the dataset and serves as a practical criterion for acceptable prediction error within the proposed framework. These findings confirm that the model is capable of reliably predicting unmeasured pigment mixtures using linear interpolation, based solely on physical $\rho(\lambda)$ data, and support its applicability in real-world subtractive colour mixing workflows.

Table 1. Quantitative evaluation of interpolation accuracy in General Sample Plane (GSP) space. Intermediate whitening mixtures (75:25, 45:55, 20:80) were excluded from the fitting process and used to validate the predictive performance of the model. ΔE values represent the Euclidean distance between predicted and measured GSP coordinates $\left(\Delta M_x(G), \Delta M_y(G)\right)$. Values below or near the reference threshold of $\Delta E \leq 1.00$ indicate high predictive reliability.

Pigment Number	Step (Pigment/White)	$\Delta \boldsymbol{M}_{\boldsymbol{x}}(\boldsymbol{G})$	$\Delta \boldsymbol{M}_{\boldsymbol{y}}(\boldsymbol{G})$	ΔE
#7. Light Green	75/25	0.45	-0.45	0.64
	45/55	0.66	-0.66	0.93
	20/80	-0.15	0.15	0.22
#18. Dark Ultramarine Violet	75/25	-0.22	-0.20	0.30
	45/55	-0.55	-0.50	0.74
	20/80	0.27	0.24	0.36
#32. Transparent Pink Earth	75/25	-0.55	0.40	0.68
	45/55	-0.87	0.64	1.08
	20/80	-0.54	0.40	0.67
#37. Cadmium Orange Yellow	75/25	-0.19	0.03	0.19
	45/55	0.38	-0.07	0.39
	20/80	-0.79	0.15	0.80

5. Discussion

Understanding the behaviour of pigment mixtures and their interaction with white pigment is fundamental to accurately modelling and predicting colour appearance in materials such as paints, coatings, and artistic media [19]. Traditional approaches often treat colour mixing and whitening as separate processes [8], yet their combined effect plays a crucial role in determining the final visual outcome. To avoid any perceptual bias or ambiguity, this study considers only the $\rho(\lambda)$ of the samples, ensuring a purely physical and objective basis for analysis. A mathematical framework is proposed to analyse and characterize whitening series and pigment mixtures within a chromatic space, using a defined reference white point as the central anchor. By establishing consistent parameters across linear whitening trajectories, the model seeks to bridge the gap between theoretical colour representation and practical application. The physically grounded nature of the proposed coordinate system offers notable advantages for practical applications in fields such as pigment formulation, colour matching, and digital rendering. In contrast to perceptual colour palettes [20], which are inherently non-linear and dependent on standardized observer models, this framework enables accurate interpolation between pigment mixtures due to its intrinsic linearity. This characteristic is particularly relevant for subtractive colour workflows, where accurately predicting colour mixtures remains a significant challenge across domains such as cultural heritage [21], ceramics [22], textile dyeing [23], and spot

colour reproduction [24]. Furthermore, the model streamlines the predictive process by operating exclusively on measurable ρ(λ), without relying on pigment-specific optical constants or assumptions related to human vision. Although perception-independent by design, the outputs of the model can be transformed into perceptual colour spaces for visualization, making it applicable as a physically accurate predictive layer compatible with existing rendering and display systems [25,26]. As such, the model complements, rather than replaces, traditional colorimetric frameworks, providing a reproducible, observer-independent basis for modelling subtractive colour behaviour. From a practical standpoint, the system could be integrated into formulation software for painting materials, digital pigment databases, or automated mixing technologies, functioning as a spectral prediction engine that enhances physical fidelity while maintaining visual interoperability. This makes it particularly valuable in contexts such as the digital cataloguing of historical pigment palettes, virtual reconstruction of degraded artworks, or predictive modelling in art conservation. Additionally, for contemporary artists or conservators working with non-traditional pigment combinations, the model offers a reliable tool for anticipating chromatic outcomes based solely on ρ(λ) measurements, thereby expanding experimental possibilities while maintaining optical control.
A performance comparison can be made given the analysis made in Figures 6 and 7, showing the improvement in the linear estimation from perception model to the one introduced in the present work.

The results presented in our work align closely with the current scientific understanding of pigment mixing in turbid media and reinforce the limitations and opportunities previously documented in pigment modelling, while remaining detached from perception-based estimations [27]. Notably, the model proposed by Moghareh Abed and Berns [8] extends the traditional one-constant Kubelka-Munk (1-KM) theory by introducing the impurity index p, effectively enhancing its applicability across a wider range of pigment mixtures, including masstones. This 1p-KM model preserves the simplicity and computational efficiency of 1-KM, while improving its accuracy for chromatic pigments that exhibit strong absorption and scattering characteristics [9,28].

In comparison to traditional two-constant KM (2-KM) models, also employed in the restoration and reconstruction of historic paintings [29], the 1p-KM theory offers a compromise between physical fidelity and computational efficiency. A previous study, based on 28 artist acrylic paints, found that although 2-KM yielded the best spectral and concentration estimations overall, 1p-KM significantly reduced estimation error compared to 1-KM, particularly for paints dominated by scattering like Yellow Ochre and Raw Sienna [8,28]. These findings underscore the importance of integrating physically meaningful corrections, like the described impurity index p, to improve prediction models based on linearity in K/S space.

Our proposed approach differs from KM-based models in that it does not rely on absorption and scattering constants, but instead utilizes integrals derived directly from $\rho(\lambda)$ data. However, it addresses similar goals like enabling linear predictions of pigment behaviour in mixtures and whitening sequences. The results of our coordinate-based system $\left(G, M_x(G), M_y(G)\right)$ demonstrate linear trajectories in chromatic space that mirror those observed in 1p-KM or 2-KM models, suggesting that the graphical method introduced here could serve as an alternative or complementary strategy to existing KM frameworks, especially for applications where physical parameters like scattering coefficients are unknown or inaccessible.

Moreover, while the impurity index p in the 1p-KM model attempts to account for the spectral impact of pigment scattering, our model inherently captures this variation through the shape of the $\rho(\lambda)$ spectrum, from which $\left(I_x(G), I_y(G)\right)$ and mixture projections $\left(M_x(G), M_y(G)\right)$ are derived. Besides, Yang and Wan [30] also addressed the issue of pigment particle size by developing a theoretical model grounded in optical principles and the physical characteristics of pigment particles. They proposed that variations in particle size affect two key types of light behaviour: surface-diffuse reflection and body-diffuse reflection. Their model demonstrated how these changes influence surface appearance, colour coordinates, and the path light travels through the medium [30]. As such, our model avoids the need to explicitly separate absorption and scattering, which may be advantageous in digital workflows or high-throughput imaging applications, such as pigment mapping in large artworks or automated pigment formulation systems [8].

Given the similarities in predictive behaviour between the two models, a future direction could involve recasting the *impurity index p* in terms of graphical intensity projections, potentially linking the conceptual domains of K-M theory and the integral-based proposed method. Additionally, the error patterns observed in the 1p-KM model for dark masstones like Phthalo Blue and Carbon Black [8] correspond to the same challenge we encountered in modelling low-reflectance samples. This suggests that both models converge in their limitations, particularly when $\rho(\lambda)$ values fall below the threshold of measurement accuracy.

Further integration of these approaches could also enhance pigment identification algorithms, leveraging the linearity and simplicity of our coordinate system with the material fidelity of KM-based methods. This would be particularly beneficial in cultural heritage imaging, where accuracy, speed, and non-invasive techniques are critical [8].

The theory presented in the current work also provides a method for characterizing objects, offering an independent approach to obtaining colour coordinates from the reflectance spectrum, as opposed to relying on more complex methods derived from existing theories, such as the use of multi-flux models [31,32].

5.1. Whitening Model Analysis

From our defined parameters, it has been demonstrated that the integral over the entire spectrum, defined as $g(\lambda)$, is null. This makes it impossible to simultaneously use $I(G)$ values calculated from each half of the spectrum, since the spectral intervals must be treated separately. For example, representing an $I(G)$ from the wavelength interval [400,550] against one from [550,700] consistently results in a slope of -1 for any mixture, indicating that no plane can exist under such conditions. An attempt was made to define three $I(G)$ over 100 nm intervals to construct a volume, but this approach was unsuccessful.

The mathematical process described involves the use of derivatives of parameters extracted from the $\rho(\lambda)$, which initially suggested a possible relationship between these parameters and those obtained directly from the derivative of the spectrum itself [33]. However, this approach did not produce any meaningful results and was ultimately discarded.

Regarding the estimations based on the white point, unlike the other pigments used, it may deviate from the trend defined by the second-degree polynomial fit. This deviation can be attributed to the fact that the white sample is not perfectly neutral; as shown by its $\rho(\lambda)$ measurements, it has likely shifted toward a yellowish appearance [34]. To resolve this issue, it was initially proposed to exclude

the white reference and instead estimate the $I_{x,y}^{W}$ values corresponding to the white point based on the data series itself. This analysis was carried out across different whitening processes, yielding varying values, which ideally should not occur if the white reference were consistent. Nonetheless, the relationship between $M(G)$ and G remained isomorphic, with no significant improvement achieved. Furthermore, using the coloured sample immediately prior to pure white as a reference for defining the curve and its tangent in each whitening series was not a viable option, as it is essential to maintain a common white reference in all cases. This ensures that white remains the central axis of the system and preserves linearity with respect to it. A case in which $(I_x^W(G), I_y^W(G))$ = (0,0) is used as the reference, instead of the actual white point corresponding to the sample, could be analysed in future studies.

Finally, the interpolation validation using unmeasured pigment-white mixtures further reinforces the predictive robustness of the GSP framework. The low ΔE values observed across all cases confirm that the coordinate system preserves linearity even beyond fitted data points. This behaviour distinguishes the model from perceptual spaces, where intermediate mixtures often follow non-linear trajectories, and highlights its suitability for physically grounded tasks such as pigment formulation and digital reconstruction workflows.

6. Conclusions

Despite the overall effectiveness of the proposed model, several limitations were encountered during its application. A subset of samples could not be included in the final representation due to reflectance inconsistencies, degradation effects, or preparation anomalies that led to deviations from expected behaviour. These issues compromised their accurate mapping within the defined chromatic plane or volume and limited the uniform application of the model across all pigment mixtures. Nevertheless, the methodology proved robust in most cases.

The reflectance-based calculation process developed for opaque paints on canvas enabled the construction of a linear, perception-independent representation system for subtractive mixing. Grounded in physical spectral data rather than perceptual colour spaces, the model allows for reliable linear combinations of pigment colours and accurate predictions of both mixing and whitening outcomes. While not intended to replace perceptual systems, this framework offers a physically robust foundation that can be integrated into existing pipelines to improve mixture prediction accuracy. Whitening, treated as a progressive mixture with a white pigment, showed particularly consistent behaviour, owing to the strength of the mathematical formulation. The coordinate system introduced, based on the parameter set $(G, M_x(G), M_y(G))$, derives directly from the $\rho(\lambda)$ curve and supports the computation of a perception-independent space. Although other chromatic centres could theoretically be used in future studies, the white reference proves to be the most suitable sample for this first approach. Despite the limitations affecting a subset of the samples, the model presents a promising framework for the quantitative analysis of subtractive colour mixing and whitening phenomena in pigment-based systems. Quantitative validation of interpolation accuracy demonstrated that unmeasured pigment mixtures could be reliably predicted within the proposed GSP space. This outcome confirms that the model not only meets its theoretical objective of linearity but also provides practical utility for accurate colour estimation in real-world subtractive mixing scenarios.

The calculations performed have demonstrated optimal performance within the scope of the tests conducted in this study; however, expanding the spectral dataset and potentially redefining some parameters may be necessary to explore alternative approaches. Future work will focus on broadening the spectral database, evaluating the system with recently applied paints, investigating the painting process itself, and assessing the effects of aging on the samples.

Additionally, the mixing behaviour of lighter colours, which has not yet been addressed, warrants thorough examination. Attention should also be given to darker colours, with the aim of obtaining more precise spectral measurements and achieving clearer discrimination among dark blues, purples, and black, colours that already challenge visual perception, especially since their tonal differences mainly emerge during the whitening process. Finally, it is anticipated that the chromatic volume will ideally converge towards a peak at the lower end of the G axis, similar to the behaviour observed with the white reference.

Finally, while the present work primarily focuses on establishing the theoretical foundation and predictive accuracy of the GSP framework, as demonstrated by the low interpolation errors reported, a more comprehensive quantitative analysis of computational efficiency and complexity, including systematic benchmarking against alternative models and semi-empirical approaches, will be addressed in future work.

Conflicts of interest. There are no conflicts to declare.

Declaration of generative AI and AI-assisted technologies in the writing process. During the preparation of this work the authors used ChatGPT by OpenAI in order to refine academic language, improve structural coherence, and align the manuscript with conventional research reporting standards. After using this tool/service, the authors reviewed and edited the content as needed and take full responsibility for the content of the publication.

Funding sources. This research did not receive any specific grant from funding agencies in the public, commercial, or not-for-profit sectors.

7. References

[1] Kubelka P, Munk F. An article on optics of paint layers. Z Tech Phys 1931;12:259–74.

[2] Kubelka P. New contributions to the optics of intensely light-scattering materials. Part I. J Opt Soc Am 1948;38:448–57.

[3] Kubelka P. New contributions to the optics of intensely light-scattering materials. Part II: Nonhomogeneous layers. J Opt Soc Am 1954;44:330–5.

[4] Zhao Y, Berns RS. Predicting the spectral reflectance factor of translucent paints using Kubelka-Munk turbid media theory: Review and evaluation. Color Res Appl 2009;34:417–31.

[5] Allen E. Basic equations used in computer color matching. J Opt Soc Am 1966;56:1256–9.

[6] Allen E. Basic equations used in computer color matching, II. Tristimulus match, two-constant theory. J Opt Soc Am 1974;64:991–3.

[7] Wyszecki G, Stiles WS. Color science: concepts and methods, quantitative data and formulae. vol. 40. John wiley & sons; 2000.

[8] Moghareh Abed F, Berns RS. Linear modeling of modern artist paints using a modification of the opaque form of Kubelka-Munk turbid media theory. Color Res Appl 2017;42:308–15.

[9] Berns RS. A generic approach to color modeling. Color Res Appl 1997;22:318–25.

[10] ISO/CIE 11664-4:2019. Colorimetry. Part 4: CIE 1976 Lab Colour space. International Organization for Standardization / International Commission on Illumination, Geneva, Switzerland; 2019.

[11] ISO/CIE 11664-3:2012. Colorimetry. Part 3: CIE tristimulus values. International Organization for Standardization / International Commission on Illumination, Geneva, Switzerland; 2012.

[12] ISO/CIE 11664-2:2020. Colorimetry. Part 2: CIE standard illuminants. International Organization for Standardization / International Commission on Illumination, Geneva, Switzerland; 2020.

[13] ISO/CIE 11664-1:2007. Colorimetry. Part 1: CIE standard colorimetric observers. International Organization for Standardization / International Commission on Illumination, Geneva, Switzerland; 2007.

[14] Di Tommaso S, Bousquet D, Moulin D, Baltenneck F, Riva P, David H, et al. Theoretical approaches for predicting the color of rigid dyes in solution. J Comput Chem 2017;38:998–1004.

[15] Tran Thl, Berraud-Pache R, Jaber M. In-silico color prediction process for natural dyes in Madder. Dyes and Pigments 2025:112701.

[16] Aporta J, Molina A. El color en las mezclas de luces frente al color de las mezclas de pigmentos y tintes. Congreso Nacional del Color, Jarandilla de La Vera, Cáceres: 1997.

[17] Aporta J, Molina A. El color en las pinturas cubrientes: nuevo diagrama de muestras. Congreso Nacional del Color, Granada: 1994.

[18] IEC 61966-2-1:1999/Amd1:2003. Multimedia systems and equipment. Colour measurement and management. Part 2-1: Colour management. Default RGB colour space, sRGB. International Electrotechnical Commission (IEC), Geneva, Switzerland; 2003.

[19] Cavaleri T, Giovagnoli A, Nervo M. Pigments and Mixtures Identification by Visible Reflectance Spectroscopy. Procedia Chem 2013;8:45–54.

[20] Gao Y, Liang J, Yang J. Color Palette Generation From Digital Images: A Review. Color Res Appl 2025;50:250–65.

[21] Berns RS. Digital color reconstructions of cultural heritage using color-managed imaging and small-aperture spectrophotometry. Color Res Appl 2019;44:531–46.

[22] Souper T, Morgado AC, Marques A, Silva I, Rosado L. Improving Color Mixture Predictions in Ceramics using Data-centric Deep Learning. ACM International Conference Proceeding Series 2023:221–9.

[23] Zhang J, Zhang X, Wu J, Xiao C. Dyeing recipe prediction of cotton fabric based on hyperspectral colour measurement and an improved recurrent neural network. Coloration Technology 2021;137:166–80.

[24] Moon J, Yang G, Tae H. A Study on DNN-Based Practical Model for Predicting Spot Color. Applied Sciences (Switzerland) 2023;13.

[25] Vermeulen M, Smith K, Eremin K, Rayner G, Walton M. Application of Uniform Manifold Approximation and Projection (UMAP) in spectral imaging of artworks. Spectrochim Acta A Mol Biomol Spectrosc 2021;252:119547.

[26] Liu Z, Zhao AR, Liu SL. Prediction of Fading for Painted Cultural Relics Using the Optimized Gray Wolf Optimization-Long Short-Term Memory Model. Applied Sciences (Switzerland) 2024;14.

[27] Wei C, Li J, Liu S. Applications of visible spectral imaging technology for pigment identification of colored relics. Herit Sci 2024;12.

[28] Berns RS, Mohammadi M. Single-constant simplification of Kubelka-Munk turbid-media theory for paint systems—A review. Color Res Appl 2007;32:201–7.

[29] Kirchner E, van der Lans I, Ligterink F, Geldof M, Ness Proano Gaibor A, Hendriks E, et al. Digitally reconstructing Van Gogh's Field with Irises near Arles. Part 2: Pigment concentration maps. Color Res Appl 2018;43:158–76.

[30] Yang X-L, Wan X-X. Analysis of the spectral reflectance and color of mineral pigments affected by their particle size. Color Res Appl 2020;45:246–61.

[31] Safdar M, Emmel P. Matching target color in polyolefins by estimating pigment concentrations using a four-flux model. Appl Opt 2023;62:6961–73.

[32] Joshi JJ, Vaidya DB, Shah HS. Application of multi-flux theory based on Mie scattering to the problem of modeling the optical characteristics of colored pigmented paint films. Color Res Appl 2001;26:234–45.

[33] Gueli AM, Gallo S, Pasquale S. Optical and colorimetric characterization on binary mixtures prepared with coloured and white historical pigments. Dyes and Pigments 2018;157:342–50.

[34] Groeneveld I, Kanelli M, Ariese F, van Bommel MR. Parameters that affect the photodegradation of dyes and pigments in solution and on substrate – An overview. Dyes and Pigments 2023;210.

Highlights

- A new model predicts subtractive color mixtures using only $\rho(\lambda)$ data
- Defines a perception-free coordinate system: $\left(G, M_x(G), M_y(G)\right)$
- Mixtures and whitening series follow linear paths in the new color space
- Model tested on 8421 samples including 43 base pigments and their mixtures
- No reliance on absorption/scattering constants or perceptual color spaces

Declaration of interests

☒ The authors declare that they have no known competing financial interests or personal relationships that could have appeared to influence the work reported in this paper.

☐ The authors declare the following financial interests/personal relationships which may be considered as potential competing interests: